Prediction of Elastic Properties for a Wound Oxide Ceramic Matrix Composite Material

Yuan Shi,* Neraj Jain, Raouf Jemmali, Severin Hofmann, and Dietmar Koch

Ceramic Composites and Structures, German Aerospace Center/Institute of Structures and Design, Pfaffenwaldring 38-40, 70569, Stuttgart, Germany

Stefan Hackemann

German Aerospace Center Institute of Materials Research, Cologne, Germany

This study presents enhanced studies of inverse approach of the classical laminate theory for prediction of the elastic properties of a wound oxide ceramic matrix composites material (CMC). Based on mechanical tests and microstructure analysis, elastic properties of virtual equivalent unidirectional layers were calculated. To adapt the analytical model to CMCs from different batches which show various fiber volume contents, porosities, and different fiber orientations, a scaling factor Ω was introduced with the help of modified mixing considering these specific properties. A good correlation between experimental and analytically calculated results showed in this study.

Introduction and Objective

Because of the favorable mechanical properties at high temperature and comparatively low density, ceramic matrix composites (CMCs) have become the focus of attention of material development in recent years, for example, for process technology and aerospace application.[1] Thanks to the high flexibility, net shape fabrication, and relatively low cost, the winding technique for production of complex CMC components, especially the production with stress-oriented fiber alignment and rotational symmetry axis, has been rapidly adapted in aerospace technology.[2–6] As the winding angle of each layer can be adjusted in any desired direction (from 0° to 90°) during the manufacturing process, the wound CMC components with pronounced anisotropic mechanical properties may be designed and optimized with stress-optimized fiber arrangement. Due to the variability of the fiber orientation and the lack of corresponding mechanical tests, an advanced modeling approach is required for the prediction and assessment of the elastic properties of wound CMCs. Several analytical approaches and finite element analysis have been developed and implemented for the prediction of mechanical properties of wound and braided materials, especially for fiber-reinforced composites with polymeric matrices. These meso- and microscopic methods based on the classical laminate theory (CLT) or on representative volume unit (RVU) allow a good estimation of elastic properties.[7–15] Furthermore, an inverse approach of CLT (called ILT) to determine the material behavior based on the experimental investigations of wound and braided CMCs has been discussed in.[16–18]

Compared to the previous study,[18] this present work is focusing on the prediction of elastic properties for wound CMCs with the effect of a scaling factor Ω. An inverse approach of CLT allows the computation of virtual UD elastic constants, even if such UD layers never can be produced in reality. The elastic constants are classified into different groups based on tensile and shear tests plus newly tested results under compressive load and further microstructure analysis. Considering the uncertainties from manufacturing, a scaling factor Ω with consideration of fiber volume content (*FVC*), porosity ε', and angle between fiber orientation and occurring stress is necessary for more precise revision of the predicted results. The efficiency of the model has been demonstrated by the investigation of a wound oxide CMC composite WHIPOX® (Wound HIghly Porous OXide CMC) for different batches with varied winding angle.

Modeling Approach

Due to the complex anisotropic in-plane material behavior, which is strongly dependent on the winding angle, the design of CMC components, such as WHIPOX®, which represents one variant of an oxide

*yuan.shi@dlr.de

fiber-reinforced CMC, has to be supplemented by an advanced modeling approach. To find the mechanical constants of a laminate from the individual properties of the fiber and the matrix is a challenge for CMCs. This can be explained by the lack of the required properties within the composite, especially for the matrix, because its microstructure, such as microcracks and specific matrix porosity after the complex processing, is totally different from pure matrix properties and depends on fiber orientation.

Two more concepts based on material homogenization techniques, either with unit cell model or with UD-layer model, can be used to build up geometrically identical repetitive elements for the prediction of mechanical properties of the composites. The unit cell approach includes the mixed properties of the fiber, the matrix, and the microstructure into a representative volume unit. Due to the requirement of a redefinition of varied fiber orientation, the use of unit cell model is not efficient. On the other hand, the CLT, which is based on the elastic constants of individual UD layers and the stacking sequence, has been successfully adapted for composites with polymeric matrices for the calculation of elastic modulus of the laminate. Consider a composite made of UD layers shown in Fig. 1 and each layer with a thickness t_k. The thickness of the whole laminate h can be calculated by

$$h = \sum_{k=1}^{n} t_k \tag{1}$$

Through the integration of the stress in the global in-plane coordinate system x-y (Fig. 2a) of each UD layer, the resultant force $N_{x,y,xy}$ and moment $Mo_{x,y,xy}$ can be formulated as in Eqs. (2) and (3).[19]

$$N_{x,y,xy} = \int_{-h/2}^{h/2} (\sigma_x, \sigma_y, \sigma_{xy}) \mathrm{d}z \tag{2}$$

$$Mo_{x,y,xy} = \int_{-h/2}^{h/2} (\sigma_x, \sigma_y, \sigma_{xy}) z \mathrm{d}z \tag{3}$$

where $\sigma = (\sigma_x, \sigma_y, \sigma_{xy})$ are average in-plane stresses.

With the help of the stiffness matrix $\left[\overline{Q}\right]$ for a multilayer laminate (Fig. 1), the relationship between strain $\{\varepsilon^0\}$, curvature $\{k\}$, resultant force $[N_{x,y,xy}]$, and moment $[Mo_{x,y,xy}]$ under in-plane loading can be described with Eq. (4).[19]

$$\begin{Bmatrix} N_x \\ N_y \\ N_{xy} \\ Mo_x \\ Mo_y \\ Mo_{xy} \end{Bmatrix} = f\left(\left[\overline{Q}\right], \varepsilon^o, \kappa\right) = \begin{bmatrix} \begin{bmatrix} S_{11} & S_{12} & S_{16} \\ S_{21} & S_{22} & S_{26} \\ S_{61} & S_{62} & S_{66} \end{bmatrix} & \begin{bmatrix} C_{11} & C_{12} & C_{16} \\ C_{21} & C_{22} & C_{26} \\ C_{61} & C_{62} & C_{66} \end{bmatrix} \\ \begin{bmatrix} C_{11} & C_{12} & C_{16} \\ C_{21} & C_{22} & C_{26} \\ C_{61} & C_{62} & C_{66} \end{bmatrix} & \begin{bmatrix} B_{11} & B_{12} & B_{16} \\ B_{21} & B_{22} & B_{26} \\ B_{61} & B_{62} & B_{66} \end{bmatrix} \end{bmatrix} \begin{Bmatrix} \varepsilon_x^0 \\ \varepsilon_y^0 \\ \gamma_{xy}^0 \\ \kappa_x \\ \kappa_y \\ \kappa_{xy} \end{Bmatrix} \tag{4}$$

The individual submatrices of $\left[\overline{Q}\right]$ are strain stiffness $[S]$, coupling stiffness $[C]$, and bending stiffness $[B]$. They were determined through the stiffness matrix of a single UD layer with thickness t_k:[19]

$$S_{ij} = \sum_{k=1}^{N} \left(\overline{Q}_{ij}\right)_k \times t_k \tag{5}$$

$$C_{ij} = \sum_{k=1}^{N} \left(\overline{Q}_{ij}\right)_k \times t_k \times \bar{z}_k \tag{6}$$

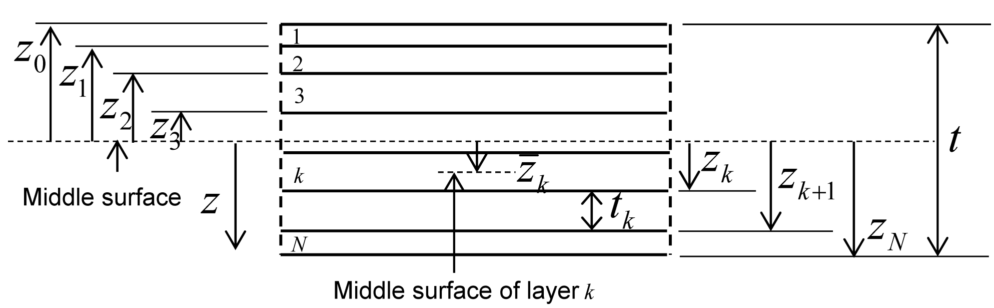

Fig. 1. Geometry of laminate plate with UD layer: the number of UD layer is from 1 to N; z_k is the distance between the middle surface of the laminate to the top or bottom of each layer; $\bar{z}_k$ is the distance between the middle surface of the laminate to the middle surface of each layer; t_k is the thickness of each layer and $t_k = z_{k+1} - z_k$.

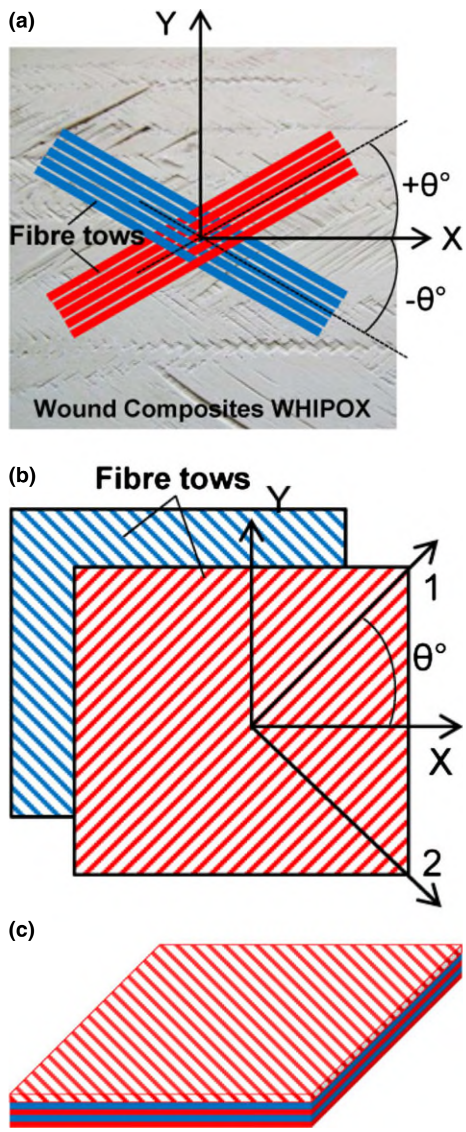

Fig. 2. Modeling approach for wound ceramic matrix composites (CMCs): (a) CMC material WHIPOX® with schematic representation of winding structure, winding angle ±θ°, and global coordinate system x-y; (b) Equivalent UD layers with local coordinate system, 1-axis in fiber direction and 2-axis in perpendicular direction; (c) equivalent composite structure with UD layers.[18]

$$B_{ij} = \sum_{k=1}^{N} \left(\overline{Q}_{ij}\right)_k \times \left(t_k \times \bar{z}_k^2 + t_k^{\,3}/12\right) \tag{7}$$

Compared to fiber-reinforced polymer composites, the modeling of mechanical properties by direct implementation of CLT is very sensitive for wound CMCs. The manufacture and characterization of characteristic CMC UD materials are almost impossible because of the nontypical unhindered shrinkage of matrix transverse to the fibers during the production process. This prevents the UD material to be considered as representative material for CLT. Therefore, an inverse approach for classic laminate theory using an equivalent UD layer is presented here with the following assumption: the material properties of the matrix are homogeneous and isotropic on a macroscopic scale; no relative movement between the fibers and the matrix exists; the residual stresses are not considered; the material exhibits linear elastic material behavior under the plane stress conditions; each single nonorthogonal wound-double-layer with wound angle ±θ° such as WHIPOX® in Fig. 2a can be replaced by two superimposed equivalent UD layers with angle +θ° and −θ° in Fig. 2b. These equivalent UD layers were defined with half the thickness of the CMC wound-double-layer and identical mechanical properties in local coordinate system by 1-axis in fiber direction and 2-axis in perpendicular direction to the fiber (Fig. 2b).

Through adaption of wound angle θ° into the inverse matrix $[Ma]^{-1}$, the material stiffness $[Q]$ in local coordinate system is derived from the transformation of the reduced stiffness matrix $\left[\overline{Q}\right]$ along the global coordinate system:[19]

$$\begin{bmatrix} Q_{11} \\ Q_{22} \\ Q_{12} \\ Q_{66} \end{bmatrix} = [Ma]^{-1} \begin{bmatrix} \overline{Q_{11}} \\ \overline{Q_{22}} \\ \overline{Q_{12}} \\ \overline{Q_{66}} \end{bmatrix} \tag{8}$$

where $[Ma]$ is the Cartesian transformation matrix and is defined as

$$[Ma] = \begin{bmatrix} m^4 & n^4 & 2m^2n^2 & 4m^2n^2 \\ n^4 & m^4 & 2m^2n^2 & 4m^2n^2 \\ m^2n^2 & m^2n^2 & m^4+n^4 & -4m^2n^2 \\ m^2n^2 & m^2n^2 & -2m^2n^2 & (m^2-n^2)^2 \end{bmatrix} \tag{9}$$

where $m = \cos\theta$ and $n = \sin\theta$

The determination of the reduced stiffness matrix $\left[\overline{Q}\right]$ requires in-plane elastic properties of a laminated composite in the global coordinate system. The terms of $\left[\overline{Q}\right]$ can be calculated from the following relations:[19]

$$\overline{Q_{11}} = \frac{E_x}{1 - \upsilon_{xy}^2 \frac{E_y}{E_x}} \tag{10}$$

$$\overline{Q_{22}} = \frac{E_y}{1 - \upsilon_{xy}^2 \frac{E_y}{E_x}} \tag{11}$$

$$\overline{Q_{12}} = \frac{E_y \upsilon_{xy}}{1 - \upsilon_{xy}^2 \frac{E_y}{E_x}} \tag{12}$$

$$\overline{Q_{66}} = G_{xy} \quad (13)$$

where E_x and E_y are the composite Young's moduli in the x- and y-directions (Fig. 2a); υ_{xy} is the laminate Poisson's ration, and G_{xy} is the laminate shear modulus.

Now, the elastic constants of the equivalent UD layer: The Young's modulus in fiber direction E_1 and perpendicular direction E_2; The Poisson's ratio υ_{12}; The shear modulus G_{12}, can be calculated with the local material stiffness $[Q]$ as follows:

$$E_1 = Q_{11} - \frac{Q_{12}^2}{Q_{22}} \quad (14)$$

$$E_2 = Q_{22} - \frac{Q_{12}^2}{Q_{11}} \quad (15)$$

$$\upsilon_{12} = \frac{Q_{12}}{Q_{22}} \quad (16)$$

$$G_{12} = Q_{66} \quad (17)$$

Finally, through the stacking of these equivalent UD layers (Fig. 2b) with the calculated elastic properties (Eqs. 14–17) and any desired fiber orientation, for example nonorthogonal, orthogonal, and unsymmetric (off-axis), an equivalent layered composite (Fig. 2c) is created and its material constants can be predicted with Eqs. (4–7).

Owing to the uncertainties created due to the manufacturing process of CMCs, the previously presented modeling approach based on CLT and inverse approach of CLT (ILT) is upgraded by introducing a scaling factor Ω, which takes into account of *FVC*, porosity (e'), and angle between fiber orientation and occurring stress. The manufacturing process of the material results in variation in the *FVC* and porosity (e') of the composite. This aspect is not included in the CLT which is required to evaluate the properties of the laminate. A relationship between *FVC*, porosity (e'), and angle between fiber orientation and occurring stress is established to predict the elastic properties of CMCs with more accuracy. With the assumption that each UD layer has identical *FVC* and the homogeneous porosity on a macroscopic scale, a linear mixing rule for the compound property can be modified to determine the scaling factor Ω_k of each equivalent UD-layer k. By the normal linear model, the compound property with influence of *Property A* and *Property B* can be formed as:

$$\begin{aligned} \textit{The compound property} &= \textit{Property A} \times \textit{Proportion of A} \\ &+ \textit{Property B} \times \textit{Proportion of B} \end{aligned}$$

The compound property (Ω_k) for elastic properties of WHIPOX® is defined by the combination of the influence of different *FVC*, e', and angle of fiber orientation between the average of the laminate and the actual values of layer k. *Property A* is the ratio of actual FVC_k of the layer to the average $\overline{FVC}$ of the laminate and *Property B* takes into consideration the ratio of the average $\overline{e'}$ to e'_k. *Proportion of A*, defined as angle between fiber orientation of the layer k and the occurring stress, is related to the *FVC*-dominated direction. On the other hand, *Proportion of B* includes the angle between the fiber orientation of the layer k to the perpendicular direction of occurring stress and is considered as the e' dominated direction. The value "$\theta_k/90$" serves as the proportion of the ratio of the porosity. Because the *Property A* and *B* together form the complete compound property with individual contributions, that is the sum of *Proportion of A* and *Proportion of B* is 100%, therefore, the value "$1 - (\theta_k/90)$" is defined for *Proportion of A*. Now, the scaling factor Ω_k can be determined with the following equation:

$$\Omega_k = \left(\frac{FVC_k}{\overline{FVC}}\right) \times \left(1 - \frac{\theta_k}{90}\right) + \left(\frac{\overline{e'}}{e'_k}\right) \times \left(\frac{\theta_k}{90}\right) \quad (18)$$

Figure 3 shows the basic curve of the scaling factor Ω_k through modified mixing rules as function of FVC_k, e'_k and angle between fiber orientation of the layer k and occurring stress. With exemplary constant values of *Property A* and *Property B*, scaling factor Ω_k showed a linear behavior to the angle between fiber orientation of the layer k to the perpendicular direction of occurring stress (*Proportion of B*). In this case, for *Proportion of B* equals to 0% is the occurring stress in fiber direction ($\theta_k = 0°$) and 100% for occurring stress perpendicular to the fiber orientation ($\theta_k = 90°$).

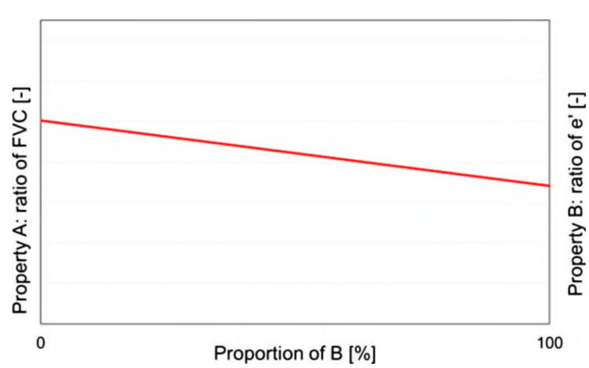

Fig. 3. Scaling factor for elastic properties through modified mixing rules as function of FVC_k, e'_k and angle between fiber orientation of the layer k and occurring stress. Computed for exemplary constant values of Property A and Property B. FVC, fiber volume content.

The scaling factor Ω_k is defined as a property of a layer in a particular laminate because it is calculated for individual layer with the consideration of the angle between the fiber orientation of the layer k and the occurring stress. After this definition, it is reasonable to use Ω_k when the layer properties are assembled into the individual submatrices strain stiffness $[S]$, coupling stiffness $[C]$, and bending stiffness $[B]$. The Eqs. (5–7) from Modeling Approach are rewritten as Eqs. (19–21). The Ω_k value is coupled with the t_k, which will lead to a more precise prediction of Young's moduli for the layer k. The engineering constants are then calculated from these new matrices.

$$S_{ij} = \sum_{k=1}^{N} \left(\overline{Q}_{ij}\right)_k \times t_k \times \Omega_k \tag{19}$$

$$C_{ij} = \sum_{k=1}^{N} \left(\overline{Q}_{ij}\right)_k \times t_k \times \Omega_k \times \bar{z}_k \tag{20}$$

$$B_{ij} = \sum_{k=1}^{N} \left(\overline{Q}_{ij}\right)_k \times (t_k \times \Omega_k \times \bar{z}_k^2 + (t_k \times \Omega_k)^3/12) \tag{21}$$

One more observation concerning to Ω_k is the calculation of the shear module G_{xy} and Poisson's ratio υ_{xy}. Both describe the material behavior between the parallel and perpendicular direction x and y for the layer k. Considering the definition of *Proportion of A* and *B* in Eq. (18), G_{xy} and υ_{xy} will be hypothesized to $(\Omega_k) \times (\Omega_k)^{-1}$, and as a result, the impact of Ω_k on G_{xy} and υ_{xy} is negligible.

Experimental

The experimental tests focus on the wound oxide ceramic composite matrix WHIPOX®. Plates with different wound angles (±3°/±87°, ±15°/±75°, ±22.5°/±67.5°, ±30°/±60°, and ±45°, 0°/90°) were manufactured at the Institute of Materials Research of the German Aerospace Center DLR in Cologne. WHIPOX® components are manufactured by a computer-controlled filament winding process with slurry infiltration of ceramic fiber bundles. The fiber roving used is 3M™ (3M, St. Paul, MN) Nextel™ (NexTech Materials, Lewis Center, OH) 610 consisting of almost pure alumina (Al_2O_3) which are embedded in a porous alumina matrix (Al_2O_3). For the mechanical tests, even plates were produced in five steps: matrix infiltration of fiber tows, computer-controlled winding with defined angle to a cylindrical moist preform, cutting and flat forming, predrying and then sintering in air and at ambient pressure for about 1 h at temperatures of approximately 1300°C.[5] The surface of a WHIPOX® plate with winding angle of ±30° is shown in Fig. 2a.

The material properties were determined and evaluated from in-plane tensile, shear (Iosipescu-method[20]), and in-plane compression tests. The samples for the experiments were cut from flat plates with fiber orientations of ±3°/±87°, ±15°/±75°, ±22.5°/±67.5°, ±30°/±60°, and ±45°, 0°/90° relative to the specimen longitudinal axis. The geometry and dimensions of specimen are shown in Fig. 4.

Tensile specimens in Fig. 4a were cut with reduced cross section in the gauge area to assure failure in the center region. For the tensile test, the longitudinal and the transverse strains were measured with strain gauges. During shear tests, the strain was evaluated from strain gauges in the +45° and in the −45° directions relative to the shear loading direction. Strain gauges for longitudinal strains were glued for compression tests. All the tests were performed at room temperature in air up to failure on an universal testing machine (Zwick, Ulm, Germany) at a controlled cross-head speed of 1 mm/min. The failure stress was calculated from the maximum load. For statistical confirmation, three to six tensile, shear, and compression samples per series were tested at room temperature.

Results and Discussion

Figure 5 shows the exemplary typical tensile, shear, and compression stress–strain curves of the investigated configurations. The longitudinal and transverse strains are presented. The indications +22.5°/−22.5° and +67.5°/

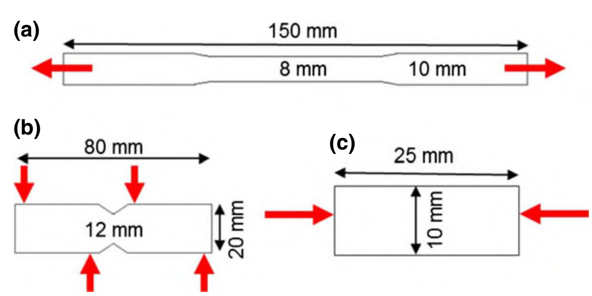

Fig. 4. Specimen geometry and dimensions used for the experiments: (a) Tensile specimen with dimensions of 150 × 10 (8) × 5 mm^3; (b) Iosipescu specimen with dimensions of 80 × 20(12) × 5 mm^3 and notch angle of 110°; (c) compression specimen with dimensions of 25 × 10 × 5 mm^3.

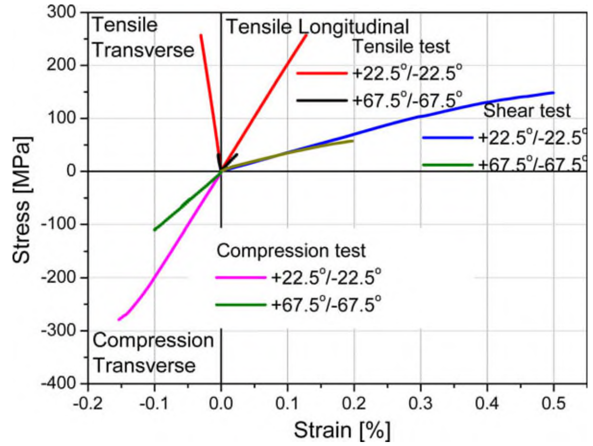

Fig. 5. Typical tensile, compression, and shear stress–strain curves for WHIPOX® with fiber orientations ±22.5° and ±67.5° from strain gauge measurement.

−67.5° denote the angles between fiber and loading direction for tensile and compression test. The stress–strain response of WHIPOX® strongly depends on the loading direction. By ±22.5° orientation and under tensile loading, the composites show an almost linear behavior with higher stiffness and strength. As the fibers are orientated close to the loading direction, the matrix is able to transfer the applied load to the fibers. In contrast, under ±67.5° tensile loading, the composite stiffness is low, and nonlinear behavior occurs even at low stresses, which indicates that damage of matrix and interface is leading to a significant degradation of the composite properties in this loading direction. The in-plane shear behavior determined through Iosipescu method is also shown in Fig. 5. The fiber orientations of the shear sample were in directions ±22.5° and ±67.5° relative to specimen longitudinal axis. As expected from CLT, the shear modulus under ±22.5° and ±67.5° loading is identical, but the shear strength of ±22.5° is much higher. Under compression loading, the Young' modulus and strength of ±67.5° are almost twice as lower as compared to the fiber orientation ±22.5°.

The elastic constants were determined using a linear fit of the initial linear region of the stress–strain curves. Some previously published elastic constants under tensile and shear loading[18] plus newly tested results under compressive load for WHIPOX® with nonorthogonal wound angle (±3°/±87°, ±15°/±75°, and ±30°/±60°) are summarized in Table I. The index X and Y correspond to the indications from Fig. 2a. The index T denotes the tensile test and C the compression test. The modeling approach for computation of equivalent UD layer described in Modeling Approach will be applied based on the experimental results in Table I.

Table I. Elastic Constants in Directions X and Y Obtained from Tensile, Shear, and Compression Tests for WHIPOX® with Different Winding Angle, the index T Denote the Tensile Test and C for Compression Test

	Batch	Test direction	FVC (%)	e' (%)	E_x^T (GPa)	E_y^T (GPa)	ν_{xy} (–)	G_{xy} (GPa)	E_x^C (GPa)	E_y^C (GPa)
Non Ortho-gonal	WF3	±3° (±87°)	42.7	22.0	214.0 ± 10.0	117.0 ± 7.0	0.19 ± 0.01	41.9 ± 0.9	–	–
	BT15	±15° (±75°)	41.2	27.9	202.0 ± 7.3	114.2 ± 3.3	0.25 ± 0.03	51.4 ± 6.9	202.3 ± 3.8	126.5 ± 14.9
	BT30	±30° (±60°)	34.0	31.4	134.4 ± 9.2	65.4 ± 9.7	0.39 ± 0.05	50.7 ± 11.4	131.0 ± 35.2	81.9 ± 7.0

To upgrade the analytical approach with consideration of scaling factor Ω (described in Modeling Approach), the average values of *FVC* and open porosity ε' from the tested composites with wound angle ±3°/±87°, ±15°/±75°, and ±30°/±60° (Table I) are summarized in Table II. The *FVC* of the samples was determined through the measurement of the initial weight of the fibers and the total weight of the component. The *porosity* of the specimens was measured using Archimedes method.[21]

To compare the test data and calculated elastic constants with consideration of various *FVC*, ε', and test directions, further experimental results from different batches with nonorthogonal (±22.5°/±67.5°, ±15°/±75° and ±30°/±60°), orthogonal wound angle (±45° and 0°/90°), and off-axis test direction (0°/60°) are summarized in Table III. The mechanical tests of the batch BR30 were conducted at the Advanced Ceramics Group, University of Bremen and the results have been taken from.[22] Same like in Table I, the index *X* and *Y* correspond to the indications from Fig. 1a. The index *T* denotes the tensile test and *C* the compression test. For orthogonally wound WHIPOX, the Young's modulus E_x is equal to E_y. Identical methods for the measurement of *FVC* and ε' from Table II have been used for the different batches, and the results are shown in Table III. Batches BT45 and BT090 were tested in different directions but prepared from the same plate; therefore, identical *FVC* and porosity ε' have been listed in Table III. Batches WF45 and WF090 were treated in the same way.

With the application of the modeling approach from Modeling Approach, the elastic parameters of an equivalent UD layer $(E_1^T, E_2^T, \upsilon_{12}, G_{12}, E_1^C, E_2^C)$ were calculated based on the experimental data from Table I for different nonorthogonal fiber orientations and under tensile and compression load. In fiber direction (1-direction), the overall mechanical response is largely determined by the properties of fibers and *FVC*. Therefore, each computed value of E_1^T and E_1^C was scaled by the average *FVC* of 39.3% in Table II.

On the other hand, in transverse direction (2-direction), the overall mechanical behavior is primarily affected by the properties of the matrix phase, which is

Table II. Average Values of Fiber Volume Content (*FVC*) and Open Porosity ε' from the Tested Composites with Wound Angle ±3°/±87°, ±15°/±75°, and ±30°/±60° in Table I

Average *FVC* (%)	Average porosity (%)
39.3	27.1

Table III. Further Mechanical Tests with Different Test Directions, *FVC* and ε', the index *T* Denote the Tensile Test and C for Compression Test

	Batch	Test direction	*FVC* (%)	ε' (%)	E_x^T (GPa)	E_y^T (GPa)	υ_{xy} (–)	G_{xy} (GPa)	E_x^C (GPa)	E_y^C (GPa)
Non ortho-gonal	WF15	±15° (±75°)	27.3	26.7	153.0 ± 3.0	96.0 ± 3.0	0.28 ± 0.01	–	–	–
	BT225	±22.5° (±67.5°)	39.1	18.5	198.4 ± 15.2	141.7 ± 13.7	0.30 ± 0.05	55.2 ± 11.9	203.5 ± 22.3	143.8 ± 19.3
	WF30	±30° (±60°)	35.3	28.3	141.0 ± 4.0	94.0 ± 4.0	0.29 ± 0.01	–	–	–
	BR30[22]	±30°(±60°)	38.6	28.4	144.9 ± 15.5	83.6 ± 5.2	0.34 ± 0.07	59.8 ± 1.5	–	–
Ortho–gonal	BT45	±45°	40.5	29.1	100.5 ± 1.1	100.5 ± 1.1	0.35 ± 0.11	59.2 ± 2.1	101.6 ± 2.3	101.6 ± 2.3
	BT090	0°/90°			122.9 ± 1.2	122.9 ± 1.2	0.12 ± 0.01	43.6 ± 8.0	152.5 ± 51.7	152.5 ± 51.7
	WF45	±45°	35.2	33.1	89.0 ± 7.0	89.0 ± 7.0	–	–	–	–
	WF090	0°/90°			105.0 ± 8.0	105.0 ± 8.0	0.08 ± 0.02	–	–	–
Off-axis	BT060	0°/60°	34.0	34.3	122.8 ± 13.6	–	–	–	–	–

FVC, fiber volume content.

related to its average porosity. E_2^T and E_2^C were scaled by ℓ = 27.1% (Table II). The calculated properties of the equivalent UD layers were used for the prediction and further comparison of elastic properties from different batches (Table III).

In contrast to the other three constants of the equivalent UD layer, the Young's modulus transverse to the fiber direction showed a strong dependence on the winding angle of tested composites, especially under tensile loading: the average value E_2^T of large angles such as ±30° and above is about only half of the ±3° or ±15°. This behavior can be explained by the shrinkage cracks observed in the matrix. During the sintering process at high temperatures, the stiff fibers block the shrinkage of the matrix. For the relative small winding angles, for example ±15°, the matrix can easily shrink in the perpendicular direction ±75° because the reinforcement of fiber in this direction is very weak. The maximum hindering of shrinkage is observed fiber orientation 0°/90° (±45°). This leads to cracking of the matrix during sintering process and thus to reduced Young's moduli in transverse direction E_2. For the analysis of shrinkage cracks, μ-computer tomography (CT) was employed for different winding angles and batches. In Fig. 6a, matrix cracks are clearly visible for the sample with orientation ±45°. To quantify the difference, the crack density will be calculated for different winding angles. In case of ±45°, the density of cracks equals approximately 8.7 per mm². In contrast, no shrinkage cracks are visible for ±22.5 orientation in Fig. 6b.

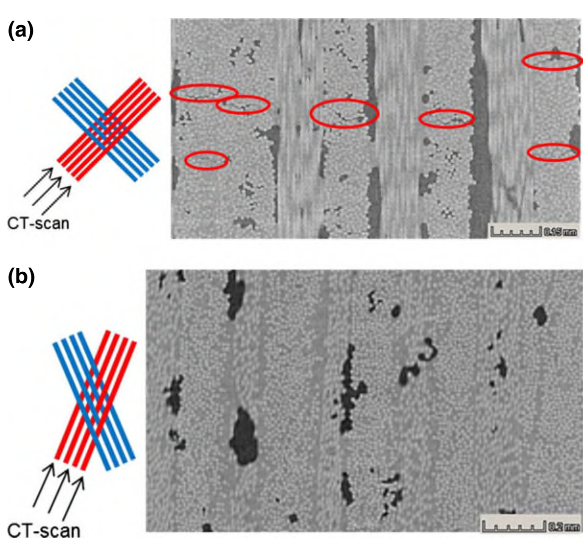

Fig. 6. CT images of the WHIPOX® material with different fiber orientations: (a) Winding angle ±45°, red marked areas show the shrinkage cracks, which are perpendicular to the fiber orientation;[18] (b) Winding angle ±22.5, there are no shrinkage cracks visible.

Further microstructure analysis results through CT for different batches with winding angle ±30° are shown in Fig. 7. Samples from batch BT30 (Table I) in Fig. 7a have similar distribution and crack density (approximately 6.7 per mm²) as ±45° in Fig. 6a. At the same time, no shrinkage cracks are observed in Fig. 6c in batch WF30 with same winding angle ±30°. Sample BR30 with crack density of approximately 2.3 pro mm² lies between these two cases, and its CT-analysis showed in Fig. 6b. WHIPOX® with same fiber orientation (±30°) but different microstructure can be explained by the effect of manufacturing fluctuations.

Discussion

In this section, the CLT and the inverse classic laminate theory are used to calculate the elastic properties of WHIPOX with different microstructure. The evaluation of scaling factor Ω using *FVC*, porosity ℓ, and angle between fiber orientation and occurring stress for the batches is explained. The effect of this factor over the prediction of material properties is discussed and compared to the original experimental results.

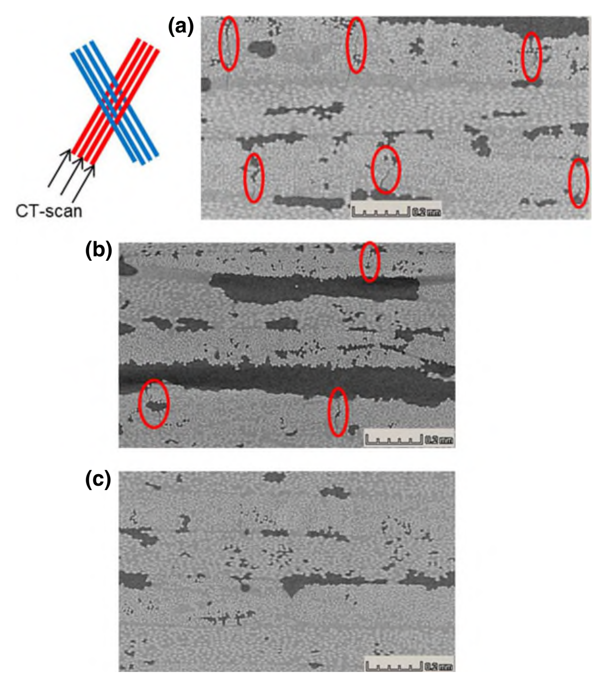

Fig. 7. Computer tomography images of the WHIPOX® material with winding angle ±30° from different batches: (a) sample BT30 similar crack density and distribution as ±45° in (Fig. 6a), (b) sample BR30 with crack density approximately 2.3 pro mm², (c) sample WF30 with no shrinkage cracks.

Based on the microstructure analysis of matrix cracks, a transition line between the matrix with and without cracks can be found by the wound angle of ±30°. No cracks were observed for smaller winding angles. WHIPOX® with winding angle of ±30° until ±45 showed similar crack distributions. Additionally, different mechanical constants under tensile and compression loading have been calculated. Therefore, the evaluation of the properties of the equivalent UD layer was divided into two classes considering the difference in fiber orientation: WHIPOX® with matrix cracks and WHIPOX® without matrix cracks. At first, each computed E_1^T and E_1^C were scaled by the average *FVC* (39.3% in Table II) of all tested specimens as fiber properties dominate the properties in 1-direction. On the other hand, E_2^T and E_2^C were scaled by the average porosity (27.1% in Table II) as the porosity has the main impact on E_2. Two UD material parameter sets with different E_1^T, E_2^T, and E_1^C, E_2^C values were defined. The UD layer parameter set UD-WC (UD layer with cracks) was defined for the angles ±45° to ±30° and a second parameter set, UD-NC (UD-layer no cracks), with higher values of E_2^T and E_2^C for the angles smaller than ±30° (Table IV). υ_{12} and G_{12} are computed from all fiber orientations for UD-WC and UD-NC. As the material showed different behavior under tensile and compression load, the Young's moduli E_1^T and E_1^C with small difference have been listed in Table IV. E_2^T and E_2^C were calculated from the respective winding angles from Table I. The E_2^T value (56.2 GPa) and E_2^C value (79.7 GPa) for UD-WC are reduced by almost 50% relative to the E_2^T under tensile (107.8 GPa) and E_2^C under compression load (124.0 GPa) from UD-NC group without microcracks.

Using the elastic constants for the equivalent UD layers of UD-WC and UD-NC in Table IV, computations were performed through CLT for symmetric wound WHIPOX composites (±θ° in Fig. 2c). The elastic constants calculated from the different parameter sets UD-WC and UD-NC under tensile and compression loading are plotted in Fig. 8 in dependence of the winding angle. Due to the changes in microstructure, a distinct turning point at ±30° can be observed by the curves in Fig. 8. E_y^T, υ_{xy}, G_{xy} and E_y^C show good agreement with the respective experimental data from Table I.

Considering the uncertainties involved during the manufacturing process, the *FVC* and ε^t can vary from WHIPOX® batch to batch, which leads to an unavoidable variation of mechanical properties, as well as the

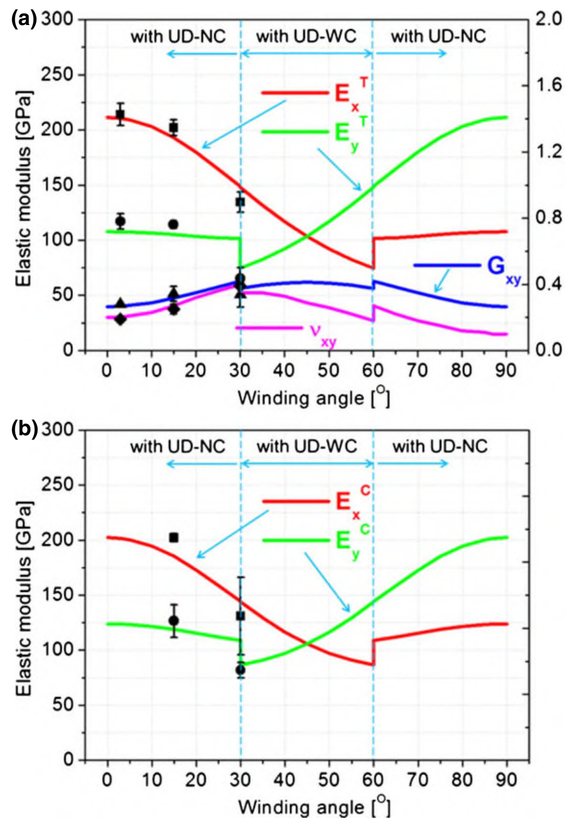

Fig. 8. Original experimental data from tensile (a) and compressive (b) tests and predicted variation of the elastic constants for wound WHIPOX® material depending on the winding angle: (a) calculated with UD properties under tensile load, (b) calculated with UD properties under compression load. Poisson's ratio υ_{xy} and shear modulus G_{xy} are identical for tensile and compression load.

Table IV. Calculated Elastic Constants for Equivalent UD Layers with Consideration of Average Fiber Volume Content and Porosity in Table II; UD-WC Corresponds to Winding Angles of ±45° to ±30°, and UD-NC Applies to Angles Smaller than ±30°

	E_1^T (GPa)	E_2^T (Gpa)	υ_{12} (–)	G_{12} (GPa)	E_1^C (GPa)	E_2^C (GPa)
UD-WC	211.2	56.2	0.20	40.0	202.4	79.7
UD-NC	211.2	107.8	0.20	40.0	202.4	124.0

Wound angle ±30° is the boundary line.

elastic constants. With the use of the method presented in Modeling Approach, scaling factor Ω was calculated with consideration of *FVC*, porosity ε', and angle between fiber orientation and occurring stress for the batches listed in Table III. The fiber orientation was symmetrical to the test direction for all tested samples. Therefore, the Ω_k for each layer is identical to the Ω for whole laminate. The results in Fig. 9 show a maximum Ω equal to 1.31 for batch BT225 in *y*-direction, which has relative low porosity (18.5%) and a minimal value of 0.73 for batch WF15 in *x*-direction due to the low *FVC* (27.3%). Ω equal to 1 means that the tested samples have same *FVC* of 39.3% and porosity ε' of 27.1% and compared to the average values in Table II. For the batch with fiber orientation unsymmetrical to test direction, the Ω_k of layer to layer can be different. In laminate BT090, the Ω_k is 1.03 in layer 0° and 0.93 for 90°. For batch WF090, the Ω_k in 0° and 90° is 0.90 and 0.82, respectively. The effect of Ω_k on the off-axis test 0°/60° is 0.87 in 0° and 0.82 in 60°.

The experimental data E_x^T and E_y^T from different batches (Table III) and predicted variation in the elastic constants under tensile load are shown in Fig. 10. The gray points by WF3 (±3°), BT15 (±15°), and BT30 (±30°) from Table I have been shown in Fig. 8 already. The black symbols for WF15 (±15°), BT225 (±22.5°), WF30 (±30°), BR30 (±30°), BT45 (±45°), and WF45 (±45°) from Table III are distributed in the area between the curves of $\Omega = 1.4$ and $\Omega = 0.6$. Following the analysis of the shrinkage cracks with the boundary line between the data sets of UD-WC and UD-NC in Fig. 7, a very good correspondence is obtained between the measured and predicted Young's moduli E_y^T in

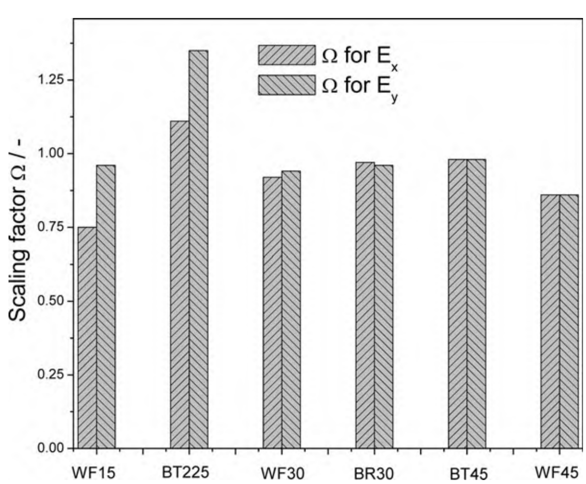

Fig. 9. Scaling factor Ω for the batches with different fiber volume content (FVC), porosity ε′, and angle between fiber orientation and occurring stress.

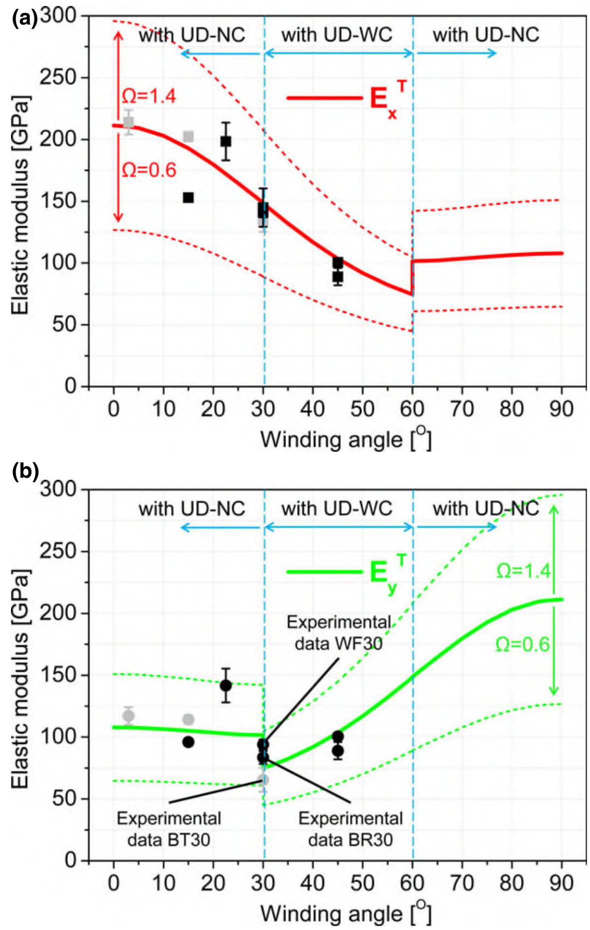

Fig. 10. Original experimental data from different batches and predicted variation of the elastic constants under tensile load with curves of $\Omega = 1.4$ and $\Omega = 0.6$ for wound WHIPOX® material depending on the winding angle: (a) calculated E_x values with UD properties, (b) calculated E_y values with UD properties.

Fig. 10b: batch WF30 without shrinkage cracks showed highest E_y^T; the Young's modulus in *y*-direction of batch BT30 with similar crack density (approximately 6.7 pro mm²) as ±45° is lowest; Sample BR30 with some cracks lies between these two batches.

Similar curves with experimental data from different batches and predicted variation of the elastic constants under compression load are plotted in Fig. 11. The gray points for BT15 (±15°) from Table I have been shown in Fig. 8 already. The black symbols for BT225 (±22.5°) and BT45 (±45°) from Table III are distributed in the area between the curves of $\Omega = 1.4$ and $\Omega = 0.6$.

The comparison of calculated elastic constants with and without consideration of Ω with the test results from Table III for wound WHIPOX® is visualized in Fig. 12.

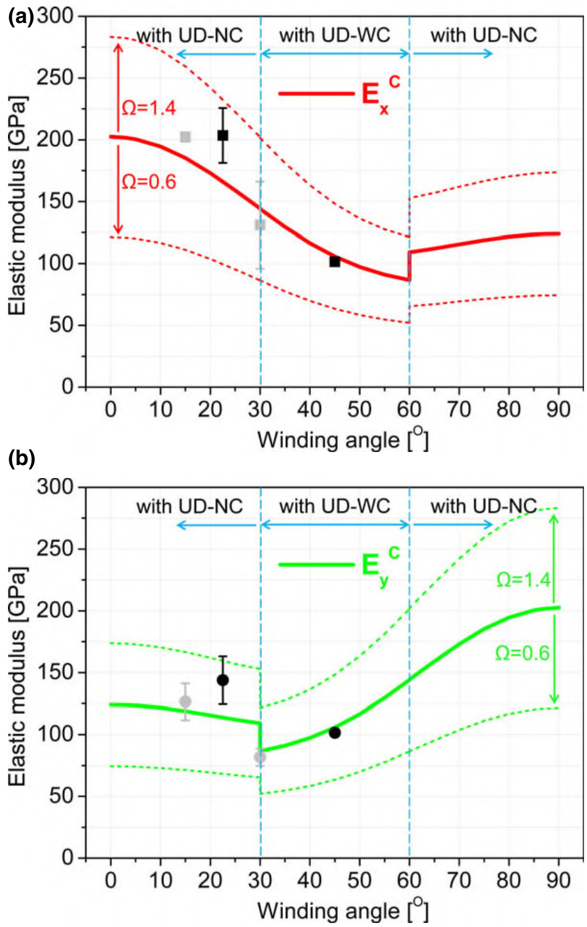

Fig. 11. Original experimental data from different batches and predicted variation of the elastic constants under compression load with curves of $\Omega = 1.4$ *and* $\Omega = 0.6$ *for wound WHIPOX® material depending on the winding angle: (a) calculated* E_x *values with UD properties, (b) calculated* E_y *values with UD properties.*

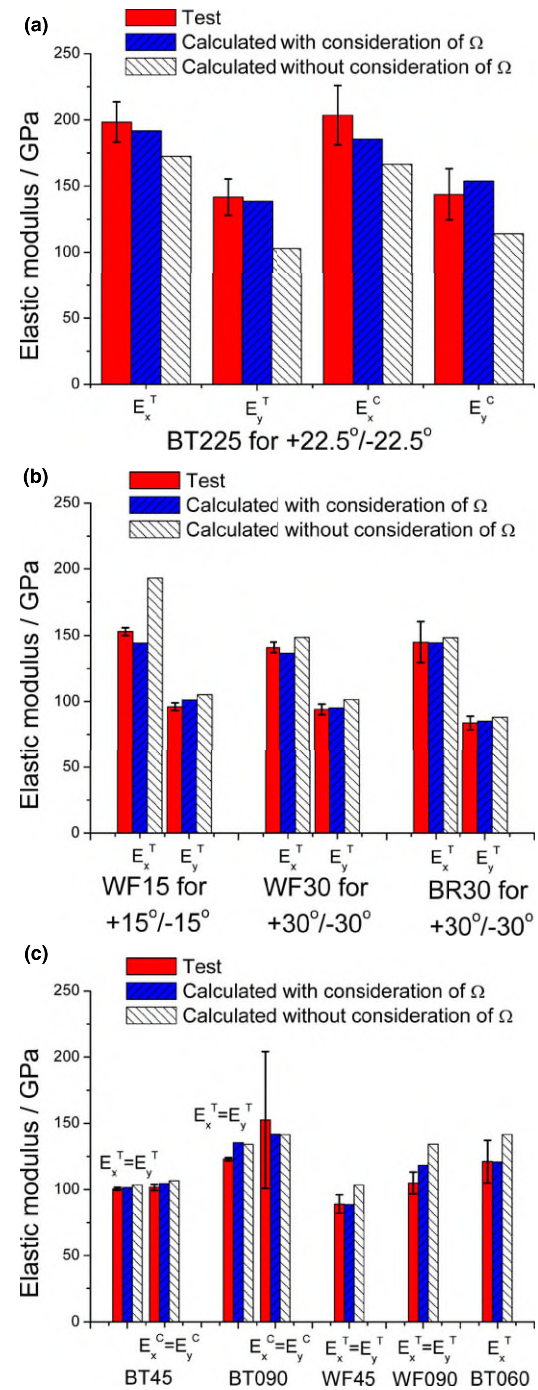

Fig. 12. Comparison of calculated elastic constants with and without consideration of Ω *to test results for wound WHIPOX® from different batches: (a) Young' modulus of nonorthogonal samples BT225 (±22.5°) under tensile and compression load; (b) Young' modulus of nonorthogonal samples WF15 (±15°), WF30 (±30°), and BR30 (±30°) under tensile and compression load; (c) Young' modulus of orthogonal samples BT45 (±45°), BT090 (0°/90°), WF45 (±45°), and WF090 (0°/90°) and off-axis test BT060 (0°/60°) under tensile and compression load.*

A very close correlation is shown in Fig. 12a–c for the measured and predicted elastic values with maximum of 12% difference by applying the scaling factor Ω. On the other hand, the computation of elastic properties without consideration of varying *FVC* and porosity $\acute{e}$ could deviate strongly from the original experimental results. For the particular batch BR30 with some shrinkage cracks, instead of using UD-WC or UD-NC properties, the average values from UD-WC and UD-NC have been applied to predict the elastic constants.

As described in Modeling Approach, the shear module G_{xy} and the Poisson's ratio υ_{xy} are calculated without consideration of Ω. Good agreement between the test results and the calculated values of G_{xy} and υ_{xy} can be observed in Fig. 13a and b.

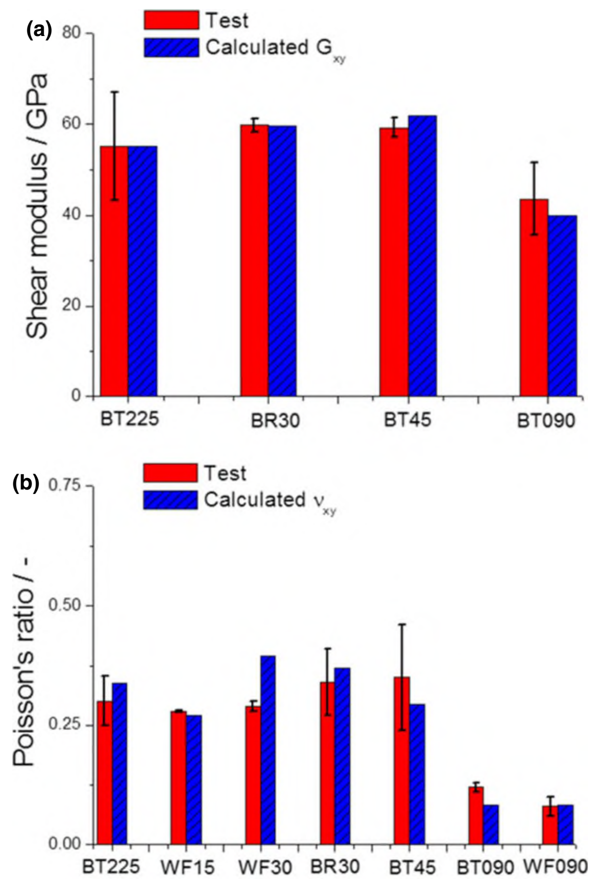

Fig. 13. Comparison of calculated elastic constants to test results for wound WHIPOX® from different batches: (a) shear modulus nonorthogonal and orthogonal samples, (b) Poisson's ratio of nonorthogonal and orthogonal samples.

Conclusions

In this study, a modeling approach with scaling factor for the prediction of elastic properties of wound ceramic composites was presented. Previously, Shi *et al.*[18] have shown that the inverse approach of CLT is suitable for the determination of the elastic properties of wound CMCs. Based on newly achieved data, this work focused on the analysis of microstructures through CT for different batches with various winding angle. Equivalent WHIPOX® UD properties under tensile and compression loading have been calculated and divided into two groups considering the fiber orientation. The boundary line between these groups was ±30°. With larger angles, microcracks in the matrix occurred; while at smaller angles, a crack free matrix was achieved. Therefore, two different UD properties were calculated via ILT, one for shrinkage crack containing matrices and one for crack free matrices. Moreover, a scaling factor Ω was introduced which considered *FVC* and porosity ε' of the different batches. The introduction of Ω was suitable to compare and interpret test results of different batches with nonorthogonal, orthogonal, and off-axis fiber orientations. By applying of the scaling factor Ω, a clearly better correlation with maximum of 12% difference between measured and predict results could be obtained. Based on the good agreement, analysis of shrinkage cracks, and modeling results, it could be shown that the modeling approach with consideration of Ω_k allows a very accurate prediction of the in-plane elastic properties for CMC laminates and will help to design and develop wound CMC structures more adequate for stiffness requirements. With this approach, a comprehensive model could be established which considers fiber orientation via ILT on the one hand side and complex and varying microstructures and material scatting via CT and microstructural analysis on the other side.

References

1. W. Krenkel, *Ceramic Matrix Composites: Fiber Reinforced Ceramics and their Applications*, Wiley-VCH Verlag GmbH & Co. KGaA, Weinheim, 2008.
2. T. P. Herbell and A. J. Eckel, *J. Eng. Gas Turbine Power*, 115 [1] 64–69 (1993).
3. S. Schmidt, S. Beyer, H. Knabe, H. Immich, R. Meistring, and A. Gessler, *Acta Astronaut.*, 55 [3–9] 409–420 (2004).
4. I. M. Low, *Ceramic Matrix Composites - Microstructure, Properties and Applications*, Woodhead Publishing, Cambridge, England, 2006.
5. J. Göring, S. Hackemann, and B. Kanka, *Mat.-wiss. u. Werkstofftech.*, 38 [9] 766–772 (2007).
6. F. Breede, R. Jemmali, H. Voggenreiter, and D. Koch, *Design and testing of a C/C-SiC nozzle extension manufactured via filament winding technique and liquid silicon infiltration*, *Conference PACRIM 10*, San Diego, USA, 2013.
7. W. Zhao, P. K. Liaw, and N. Yu, *J. Nucl. Mater.*, 253 [1–3] 10–19 (1998).
8. Z. M. Huang, *Compos. Sci. Technol.*, 60 [7] 479–498 (2000).
9. J. Carey, M. Munro, and A. Fahim, *J. Reinf. Plast. Comp.*, 22 [9] 813–831 (2003).
10. P. Potluri and A. Manan, *Compos. Part A*, 38 [4] 1216–1226 (2007).
11. L. Srikanth and R. M. V. G. K. Rao, *J. Reinf. Plast. Comp.*, 30 [16] 1359–1365 (2011).
12. L. Xu, S. J. Kim, C. H. Ong, and S. K. Ha, *J. Compos. Mater.*, 16 [18] 2255–2270 (2012).
13. H. Richter, *Numerical modelling of a ceramic matrix composite with porous matrix phase, ODAS 2013 - 13th ONERA-DLR Aerospace Symposium, Palaiseau, Frankreich*, 2013.
14. C. K. Leung, G. W. Melenka, D. S. Nobes, and J. P. Carey, *Comp. Struct.*, 100, 135–143 (2013).
15. X. B. Ji, *et al.*, *J. Compos. Mater.*, 48 [8] 931–949 (2014).
16. K. Tushtev, D. Koch, and G. Grathwohl, *Int. J. Mater. Res.*, 99 [11] 1262–1267 (2008).
17. O. Zebdi, R. Boukhili, and F. Trochu, *J. Reinf. Plast. Comp.*, 28 [23] 2911–2930 (2009).
18. Y. Shi, S. Hofmann, R. Jemmali, S. Hackemann, and D. Koch, *J. Ceram. Sci. Technol.*, 05 [1] 31–38 (2014).
19. A. K. Kaw, *Mechanics of Composite Materials*, CRC Press, Florida, 2005.
20. N. Iosipescu, *J. Mater.*, 2 537–566 (1967).
21. DIN EN 1389, *Advanced technical ceramics—Ceramic composites—Physical properties—Determination of density and apparent porosity*, 2004.
22. M. Gerendás, *et al.*, *Development and Validation of Oxide/Oxide CMC Combustors Within the HiPOC Program*, ASME Turbo Expo 2013: Turbine Technical Conference and Exposition, 4, 2013.